J. Fluid Mech. (1982), *vol.* 122, *pp.* 123–142
Printed in Great Britain

Transition from periodic to chaotic thermal convection

By JOHN B. McLAUGHLIN
Department of Chemical Engineering, Clarkson College of Technology, Potsdam, N.Y. 13676, U.S.A.

AND STEVEN A. ORSZAG
Department of Mathematics, Massachusetts Institute of Technology, Cambridge, MA 02139, U.S.A.

(Received 17 August 1981 and in revised form 5 January 1982)

The transition to turbulence in Bénard convection in a layer of air bounded by rigid conducting walls is studied by numerical solution of the three-dimensional time-dependent Boussinesq equations. The wavy instability of rolls is compared with available experimental and theoretical results. The subsequent transition to chaotic convection is shown to occur for Rayleigh numbers larger than about 9000. The role of symmetry-breaking perturbations in the production of chaos is clarified.

1. Introduction

The sequence of instabilities leading to turbulence in thermal convection between flat horizontal plates has been studied extensively. One of the nice features of this problem is that irregularity develops more slowly as a function of the driving force than it does in such shear flows as pipe or channel flow. However, it is also well known (Willis & Deardorff 1970; Krishnamurti 1973; Clever & Busse 1974, 1978; Busse & Clever 1979; Ahlers & Behringer 1978, 1979; Gollub & Benson 1980) that even the qualitative nature of the instabilities leading from a state of steady convective flow to a state characterized by a broad frequency spectrum depends on a number of factors such as the Prandtl number and the geometrical parameters of the container in which the experiments are conducted.

One must be cautious about using the word 'turbulent' to describe these freely convecting flows since this word is usually associated with high-Reynolds-number flows, such as fully developed turbulent pipe flow, in which the energy is distributed over a large range of spatial and temporal scales. The kind of convective flows which we shall discuss in this paper typically have Reynolds numbers (based on the maximum velocity and the thickness of the convection layer) of order 10–100, and have over 99 % of their kinetic energy contained in a single octave of wavenumbers. Thus one should not confuse the kind of weak turbulence which we shall discuss with, for example, the kind of strong turbulence encountered in pipe flow and analysed in the classic experiments of Laufer (1954). Nevertheless, the convective processes studied here are of interest since they give an example of one way fluid flow can become chaotic.

The results presented below tend to support the theory of Ruelle & Takens (1971) about the maximum number of independent oscillatory modes which a system can

sustain without generating broadband frequency spectra. It is worth while to describe this theory briefly in order to clarify the relationship between their work and laboratory experiments. Ruelle & Takens postulate a flow that undergoes a sequence of oscillatory instabilities as a parameter (e.g. a Reynolds or Rayleigh number) is increased. It is assumed that at low values of the parameter the only stable state of the system is a steady (laminar) flow. As the parameter is increased beyond some critical value an instability occurs in which an oscillatory mode grows exponentially. Assuming that nonlinearity has a stabilizing effect, this growing mode will eventually saturate and a time-periodic flow will result. One can then imagine that as the parameter is increased still further a second oscillatory mode appears and also saturates at some finite amplitude. Since the system is nonlinear, one expects the velocity or temperature at a given point to contain the harmonics of the two frequencies, as well as sum and difference frequencies. This is an example of a quasiperiodic system since the frequency spectrum consists exclusively of delta functions superimposed on whatever instrumental noise may be present in the given experiment.

However, if a third oscillatory mode appears when one varies the driving parameter to a higher value, Newhouse, Ruelle & Takens (1978) argue that the frequency spectrum should typically contain broadband frequency excitations. They consider motion on a three-torus (quasiperiodic motion with three basic frequencies) and then imagine introducing a small nonlinear coupling between the three oscillators. One can visualize such a system as a system of three harmonic oscillators with different natural frequencies which are initially uncoupled. They argue that it is very likely that even very weak nonlinear couplings will produce broadband components in the frequency spectrum of such a system. It should be pointed out that the fact that nonlinearly coupled oscillators typically have regions of chaotic motion even for systems of $1\frac{1}{2}$ degrees of freedom (three real variables) has been known since the work of Chirikov (1959) on Hamiltonian systems. More recently, Ford & Lunsford (1970) have shown that the introduction of arbitrarily weak couplings produces regions of chaos for a Hamiltonian system of three resonant oscillators.

It should be noted that the Ruelle–Takens theory is at variance with the traditional view expounded by Landau (Landau & Lifshitz 1959) in which quasiperiodic flows with arbitrarily large numbers of frequencies arise in a discrete manner as the forcing parameter increases.

As noted by McLaughlin & Martin (1975), the Ruelle–Takens theory is not applicable to the transition to turbulence in many flows of practical interest, including pipe or channel flows, in which nonlinearity tends to destabilize perturbations of the laminar flows. For example, according to linear theory, plane Poiseuille flow is stable at Reynolds numbers (based on the half-width of the channel) smaller than 5772 (Orszag 1971). However, Herbert (1977) has shown numerically that plane Poiseuille flow is unstable to finite-amplitude two-dimensional perturbations at Reynolds numbers as low as roughly 2900. Using three-dimensional simulations, Orszag & Kells (1980) and Orszag & Patera (1981) found the threshold for transition to be roughly 1000, which is in good agreement with laboratory experiments (see Orszag & Kells 1980). Thus nonlinear effects may drive these flows into states described by a broad frequency spectrum without the kind of intermediate stages envisaged by the Ruelle–Takens theory. Similar nonlinear instabilities appear to hold in most of the classical shear flows.

In order to find a flow that may satisfy the assumptions made in the Ruelle–Takens theory, one must find a flow that exhibits oscillatory behaviour in some parameter range. Thermal convection in air and other low-Prandtl-number fluids is such a flow (Willis & Deardorff 1970; Krishnamurti 1973; Ahlers & Behringer 1978, 1979; Gollub & Benson 1980). Willis & Deardorff performed their experiments in a large-aspect-ratio rectangular container with horizontal and vertical dimensions of 80 cm and 2·54 cm respectively. They found that for Rayleigh numbers smaller than 5800 the convection was steady except for slow undulations and that the pattern consisted of approximately two-dimensional rolls. However, when the Rayleigh number exceeded 5800 they detected three-dimensional wavy oscillations in the flow both visually and with a thermocouple. This finding was confirmed by Krishnamurti (1973), who found the threshold Rayleigh number for oscillations in air to be 5600. Clever & Busse (1974) performed a linear stability analysis for three-dimensional perturbations on two-dimensional rolls and found that for the Prandtl number of air wavy oscillations develop a positive growth rate when the Rayleigh number exceeds 6000, if the roll wavelength is chosen to match the experimental data of Willis, Deardorff & Somerville (1972).

Willis & Deardorff found that, although the time dependence of the convection is roughly periodic at Rayleigh numbers on the order of 9000, it becomes increasingly irregular as the Rayleigh number is increased, and well-defined oscillations are no longer discernible when the Rayleigh number is of order 30000. However, they did not report frequency power spectra for the temperature or velocity fields in their experiments, so it is impossible to make a detailed comparison between their results and the Ruelle–Takens theory.

Frequency spectra were measured by Gollub & Benson (1980) in their study of convection in fluids having Prandtl numbers between 2·5 and 5·0 and contained in small-aspect-ratio cells (16·42 by 27·72 by 7·90 mm high and 14·66 by 28·85 by 11·94 mm high). They found several different routes by which convective flows can become turbulent. In some cases they found that flows with broad spectra were preceded in Rayleigh number by quasiperiodic flows with two or three frequencies. In another case they found that a succession of subharmonic (periodic-doubling) bifurcations preceded the onset of broad spectra. The fact that they were able to find quasi-periodic flows with three distinct frequencies which did not contain broad spectral components cannot fairly be taken as a disproof of the Ruelle–Takens theory, since Ruelle & Takens only claim that it is probable that quasiperiodic flows with three frequencies will be ruled out by the nonlinearity in a system. The Ruelle–Takens theory is probably most usefully interpreted as a rule of thumb that broadband components will start to appear after a small number of oscillatory modes have developed in a system. However, in all our simulations reported below, solutions containing three or more distinct frequencies do contain broad spectral components.

In this paper, we report simulations of transitional thermal convection in air with the goal of identifying the modes that are responsible for the appearance of broadband spectral components. Specifically, we have been able to establish a link between the breakdown of certain spatial symmetries and the onset of chaos. Of course, one can also look for changes in the spatial symmetries in the laboratory. However, it would be difficult, if not impossible, to determine whether those changes are the cause of the chaos or whether the flow would still be chaotic even if the symmetries were somehow

enforced. The advantage of the computer in this respect is that it enables one to study the behaviour of the solutions with the symmetry-breaking variables set equal to zero. By doing this, we have found that the symmetry-breaking modes can hasten the onset of chaos.

A number of other workers have studied thermal convection using numerical simulation. The most immediately relevant work is that of Lipps (1976), who studied oscillatory convection in air using high-resolution finite-difference techniques. Lipps simulated the flow with Rayleigh numbers of 6500, 9000 and 25 000. When the Rayleigh number was 6500 the flow evolved into a time-periodic state. The flow contained at least two frequencies when the Rayleigh number was 9000, and the flow appeared to be highly chaotic when the Rayleigh number was 25000. Lipps did not integrate far enough in time to enable him to analyse the frequency content of the flows that he simulated.

Toomre, Gough & Spiegel (1977) found that, provided an adequate amount of vertical resolution was used, models of convection in which a single horizontal mode was retained exhibited no time dependence. Marcus (1981) has found a similar result in a study of convection in a spherical geometry, and he has also shown that, if several azimuthal modes are retained, a threshold for time dependence exists, but that this threshold tends to increase as the azimuthal resolution is increased (i.e. inadequate azimuthal resolution can give spurious time dependence). Curry *et al.* (1982) find that inadequate spatial resolution of two-dimensional convection gives spurious time dependence, while adequately resolved two-dimensional flows exhibit much less time dependence than real three-dimensional flows. Also, Orszag & Kells (1980) found that simulations with inadequate horizontal resolution also tend to yield spuriously low thresholds for instability of plane Poiseuille flow. Thus it is important to check carefully that both the horizontal and vertical resolution are sufficient before concluding that a simulation that exhibits chaotic behaviour implies that the corresponding exact solution of the Boussinesq equations is chaotic.

In § 2, we give a brief discussion of our numerical techniques. In § 3, we study the possible symmetries of Bénard convection. In § 4, we present our results for the onset of chaos in air and the role of symmetry-breaking perturbations in this process.

2. Numerical methods

In our three-dimensional simulations, we impose rigid no-slip boundary conditions on the two surfaces of the convection layer, and periodic boundary conditions in the two horizontal directions. The temperature is assumed to be constant on the two surfaces. The repetition lengths in the two horizontal directions are set equal to the experimental wavelengths reported by Willis & Deardorff (1970) and Willis *et al.* (1972). The fluid is assumed to satisfy the Boussinesq conditions, so that the equations of motion are

$$\frac{\partial \mathbf{v}}{\partial t} = \mathbf{v} \times \boldsymbol{\omega} - \nabla \pi + Pr(\nabla^2 \mathbf{v} + \hat{\mathbf{z}}\theta), \tag{2.1}$$

$$\frac{\partial \theta}{\partial t} + \mathbf{v} \cdot \nabla \theta = Ra\, w + \nabla^2 \theta, \tag{2.2}$$

$$\nabla \cdot \mathbf{v} = 0, \tag{2.3}$$

where $\mathbf{v} = (u, v, w)$ is the velocity field. $\boldsymbol{\omega} = \nabla \times \mathbf{v}$ is the vorticity, $\pi = p + \frac{1}{2}|\mathbf{v}|^2$ is the pressure head, with p the pressure, and θ is the deviation of the temperature from the conduction profile.

In (2.1)–(2.3), distances and times have been made dimensionless in terms of the thickness H of the layer, and the vertical thermal diffusion time $\tau_d = H^2/\kappa$, where κ is the thermal diffusivity. Here θ is made dimensionless in terms of the temperature difference ΔT between the two plates. The parameter Ra is the Rayleigh number and Pr is the Prandtl number:

$$Ra = \frac{g\epsilon H^3 \Delta T}{\nu\kappa}, \tag{2.4}$$

$$Pr = \nu/\kappa, \tag{2.5}$$

where g is the acceleration due to gravity, ϵ is the coefficient of thermal expansion, and ν is the kinematic viscosity. The Prandtl number of air is 0·71 and we have used this value in all of the simulations which are discussed below.

The velocity and temperature fields are expanded using Fourier series in the x- and y-directions, and a Chebyshev polynomial series in the vertical z-direction. Thus the fields are represented as

$$\mathbf{v}(x, y, z, t) = \sum_{|m|<\frac{1}{2}M} \sum_{|n|<\frac{1}{2}N} \sum_{p=0}^{P} \tilde{\mathbf{v}}(m, n, p, t)\, e^{2\pi i(mx/X + ny/Y)} T_p(2z), \tag{2.6}$$

$$\theta(x, y, z, t) = \sum_{|m|<\frac{1}{2}M} \sum_{|n|<\frac{1}{2}N} \sum_{p=0}^{P} \tilde{\theta}(m, n, p, t)\, e^{2\pi i(mx/X + ny/Y)} T_p(2z), \tag{2.7}$$

where X is the wavelength of the rolls and Y is the wavelength of the waves that develop on the rolls. Here $T_p(z)$ is the Chebyshev polynomial of degree p. Also, M, N, P are spectral cutoffs typically chosen to be $M = 16$, $N = 16$, $P = 16$ in the calculations reported below.

In all the simulations reported in this paper, X is chosen equal to the experimental value of the roll wavelength, as reported by Willis *et al.* (1972). The z-co-ordinate varies between $-\frac{1}{2}$ and $+\frac{1}{2}$. Equations for the spectral components of the fields are obtained using the pseudospectral method described by Orszag & Kells (1980).

One essential feature of the present code is the use of Richardson extrapolation to reduce time-stepping errors. Time stepping is performed by a fractional-step (splitting) method in which the fractional steps involve (i) the nonlinear advection and linear buoyancy terms; (ii) the pressure to enforce incompressibility; and (iii) the viscous terms to enforce the rigid boundary conditions. Since the operators involved in these three substeps do not commute, time-stepping errors $O(\Delta t)$ result even if the local error in each substep is smaller. Local Richardson extrapolation reduces this error substantially: If $\mathbf{v}_1(\Delta t)$ is the first-order result that obtains from splitting then

$$\mathbf{v}_2 = 2\mathbf{v}_1(\tfrac{1}{2}\Delta t) - \mathbf{v}_1(\Delta t) \tag{2.8}$$

removes the first-order error†.

The code has been tested in several ways. First, the time evolution of small-amplitude perturbations of the pure-conduction state (no motion) has been computed using the

† *Note added in proof:* the error in $\mathbf{v}_2$ is $O(\Delta t^{\frac{3}{2}})$.

Method	Δt	Rayleigh number 3000	6000	10000
Exact	—	1·867 90	5·048 43	8·230 29
No Richardson extrapolation	0·003 00	1·928 50	5·111 24	8·294 74
	0·001 50	1·899 10	5·081 29	8·264 94
	0·000 75	1·883 77	5·065 27	8·248 30
Local Richardson extrapolation	0·003 00	1·871 63	5·052 60	8·233 41
	0·001 50	1·869 27	5·050 08	8·231 85
	0·000 75	1·868 40	5·049 05	8·230 95

TABLE 1. Computed growth rates $\mathscr{R}(\sigma)$ for the most unstable mode as a function of time step (here we calculate $\mathscr{R}(\sigma)$ using $M = 8, P = 16, \alpha = 2\pi/X = 1{\cdot}5585$)

M	P	Nu
4	8	3·286
4	16	3·241
4	32	3·240
16†	16†	3·258†

† Clever & Busse (1974).

TABLE 2. Steady-state Nusselt numbers at $Ra = 2000$

exact linear eigenfunctions (that evolve as $e^{\sigma t}$) as initial conditions. The growth rate as computed from the time evolution of the perturbation is then compared with the exact eigenvalue, using various vertical resolutions P and time steps Δt. The results show that, for fixed time step Δt, the growth rate changes by less than 1 % when P increases from 8 to 32 when $Ra \lesssim 20000$. Also, as documented in table 1, without Richardson extrapolation in time, the error in the (large-P) growth rate $\mathscr{R}(\sigma)$ behaves like Δt. Richardson extrapolation (2.8) at each time step reduces this error considerably.

In order to check the accuracy of the Chebyshev series used for the vertical representation of the flow, we performed a number of two-dimensional simulations. In table 2, we give the values of the steady-state Nusselt number for $M = 4$ and $P = 8$, 16 and 32, and compare our values with Clever & Busse's (1974) value for the same parameter values. Clever & Busse's value may be more accurate than ours since they used more horizontal resolution than we did, and their vertical resolution should be sufficient to give accuracy as good as ours.

We used the linear stability results of Clever & Busse (1974) for three-dimensional perturbations as a further check of our code. Specifically, Clever & Busse found that, when they used the experimental results of Willis & Deardorff (1970) for X, the oscillatory mode became unstable when $Ra = 6000$ and $Y = 2{\cdot}5$ (the most unstable mode). Using these values for X and Y, we found that the wavy perturbation was damped for $Ra = 6100$ and unstable for $Ra = 6200$. Our results are summarized in table 3. The small discrepancy between our value for the threshold and the value found by Clever & Busse is almost certainly due to the low horizontal resolution used in our simulations ($M = 4$). Our simulations used $P = 32$ for the vertical resolution.

Finally, several tests of the horizontal resolution used in our simulations have been

Rayleigh number	X	Y	Growth rate $\mathscr{R}(\sigma)$	$\mathscr{I}(\sigma)$
6100	2·85	2·5	−0·13	23·0
6200	2·85	2·5	0·084	23·0

TABLE 3. Eigenvalues σ near the oscillatory threshold found by full simulation

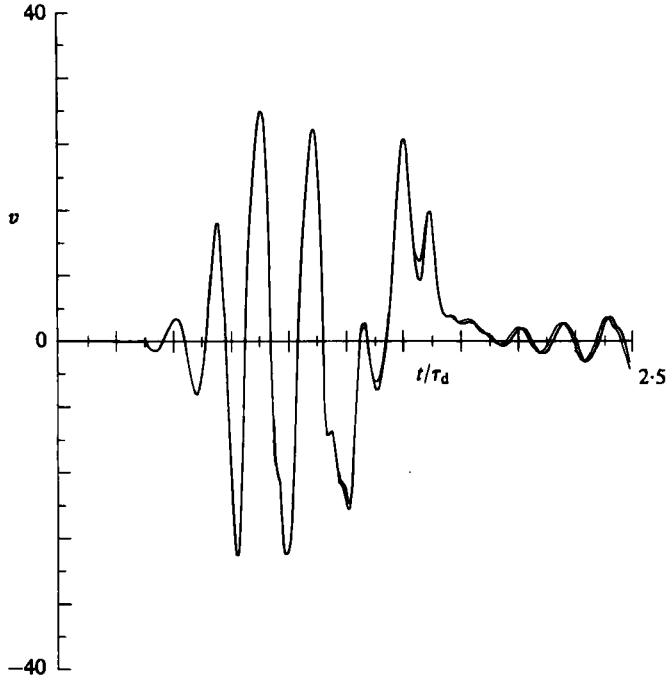

FIGURE 1. Effect of horizontal evolution on the time evolution of a velocity component for the run at $Ra = 15000$. Heavy curve: $M = N = 8$, $P = 32$, Light curve: $M = N = 16$, $P = 32$.

made at the larger Rayleigh numbers. It has been found that simulations using $M = N = 4$ and $P = 16$ or 32 fail badly for $Ra = 15000$ in that their time dependence is not even qualitatively correct. Noticeable qualitative differences between $M = N = 8$ and $M = N = 16$ begin to develop for Ra of order 25000. In figure 1, we compare the time evolution of the y-component of velocity at a point in the middle of the convection layer for simulations using $M = N = 8$, $P = 32$ and $M = N = 16$, $P = 32$ with $Ra = 15000$. In these runs $X = 3{\cdot}78$ and $Y = 2{\cdot}65$. It can be seen that the two time evolutions are quite close except for a slight phase shift. This run provides a severe resolution test, as the rolls flip orientation in their time evolution. Similarly, we believe that the accuracy of all the simulations reported below is sufficient. While the 'chaotic' flows reported below may not be accurate in phase at large times, a qualitative application of the Anosov–Bowen shadow lemma (see Lanford 1982) suggests that the reduced data obtained from the numerical simulations are the exact reduced data for some modified initial flow close to that imposed in the calculation.

It is important to emphasize the limitations imposed on our simulations by the assumption of periodic boundary conditions in the horizontal directions. The repetition

lengths are set equal to the wavelengths of the rolls and waves that were observed by Willis & Deardorff (1970). In doing so, all of the larger-wavelength (subharmonic) fluctuations which are apparently seen in experiments using large-aspect-ratio containers are eliminated. Therefore it is not surprising that the behaviour that we find is qualitatively similar to the phenomena observed in small-aspect-ratio containers. On the other hand, it is dangerous to attempt a quantitative comparison with such experiments, since the effects of no-slip side walls are not included in our simulations. Also, with our horizontal periodic boundary conditions the effects of such instabilities as the skewed varicose instability (Busse & Clever 1979) are not accounted for. Their inclusion would require much larger horizontal repetition lengths and consequently significant loss of horizontal resolution.

3. Flow symmetries

There are several symmetries which are consistent with (2.1) and (2.2). For example suppose the convection takes the form of two-dimensional rolls aligned parallel to the y-axis. Then the flow has translational invariance in y, and the x- and z-components of velocity and the temperature satisfy the following reflection symmetries with respect to x:

$$u(-x,z,t) = -u(x,z,t), \tag{3.1}$$

$$w(-x,z,t) = w(x,z,t), \tag{3.2}$$

$$\theta(-x,z,t) = \theta(x,z,t). \tag{3.3}$$

However, Clever & Busse (1974) have shown that these two-dimensional roll solutions become unstable to three-dimensional wavy perturbations when the Rayleigh number exceeds 6000. Clearly, this breaks the translational invariance in the y-direction. However, it also breaks the reflection symmetry in the x-direction.

It is possible to set up a standing-wave solution in the y-direction by imposing the following reflection symmetries on the velocity and temperature fields:

$$u(x,-y,z,t) = u(x,y,z,t), \tag{3.4}$$

$$v(x,-y,z,t) = -v(x,y,z,t), \tag{3.5}$$

$$w(x,-y,z,t) = w(x,y,z,t), \tag{3.6}$$

$$\theta(x,-y,z,t) = \theta(x,y,z,t). \tag{3.7}$$

Numerical calculations show that these standing-wave solutions are time-periodic up to $Ra = 25000$ approximately, and that the periods are in good agreement with those reported by Willis & Deardorff (1970). However, the simulations show that these solutions are unstable with respect to travelling-wave disturbances that break the y-symmetries (see also Lipps 1976).

In order to generate the symmetrized solutions, initial conditions are chosen that are consistent with the symmetries (3.4)–(3.7). These continuously yield finite-amplitude solutions with the desired symmetries that persist for at least two thermal diffusion times (which corresponds to roughly eight oscillation periods over the range of Rayleigh numbers where the standing-wave solutions are time-periodic). However, in long-time simulations (38 thermal diffusion times), the symmetry is broken by the end of the run. The source of the initial symmetry-breaking perturbations is round-off errors (of order 10^{-14} in our runs on the CRAY-1); amplification rates for the

symmetry-breaking modes are such that these variables attain finite amplitudes in roughly five to ten thermal diffusion times for most of the Rayleigh numbers studied.

One can impose a more subtle symmetry, which we shall refer to as 'spectral parity'. It is possible to find solutions that satisfy the following conditions on the modal indices:

$$\tilde{u}(m,n,p,t) = \tilde{v}(m,n,p,t) = 0 \quad \text{unless } m+p \text{ is even}, \tag{3.8}$$

$$\tilde{w}(m,n,p,t) = \tilde{\theta}(m,n,p,t) = 0 \quad \text{unless } m+p \text{ is odd}. \tag{3.9}$$

For example, two-dimensional rolls aligned parallel to the y-axis satisfy these spectral-parity conditions (Clever & Busse 1974) for Rayleigh numbers sufficiently close to the convective threshold. The oscillatory mode that bifurcates at $Ra = 6000$ also satisfies spectral parity.

However, for $Ra > 9000$, solutions that have spectral parity are unstable with respect to symmetry-breaking modes. Furthermore, the symmetry-breaking modes are important in the production of broadband frequency components. In order to detect such modes, one can print out their values or one can test for a spatial symmetry which fields satisfying spectral parity must possess. Specifically, it can easily be shown that, when spectral parity holds, in the middle of the convection layer (i.e. the plane $z = 0$) w and θ are invariant under translations by $\frac{1}{2}X$ in the x-direction, while u and v change sign. In § 4, we present contour plots of the fields in the plane $z = 0$ in order to demonstrate the presence or absence of spectral parity.

4. Results

Let us begin by reporting a series of simulations in which standing waves are established by imposing (3.4)–(3.7) on the initial conditions. As mentioned previously, for each Rayleigh number the periodicity length X was set equal to the experimentally measured roll wavelength reported by Willis *et al.* (1972). Willis & Deardorff (1970) observed that the wavelength of the waves was approximately 0·7 that of the rolls in the vicinity of $Ra = 9000$. Therefore, in most of the standing-wave simulations we assume $Y = 0{\cdot}7X$ (with X given by the experiments), even though experimental values are not available for Y except at $Ra = 9000$. We also performed simulations with different values of Y at a few Rayleigh numbers in order to check that the motion is indeed not qualitatively different.

In these standing-wave simulations, nearly steady two-dimensional rolls parallel to the y-axis are generated by using the eigenfunctions for the convective threshold as initial conditions with a finite amplitude and integrating for τ_d (where τ_d is the vertical thermal diffusion time). Then, a finite-amplitude three-dimensional disturbance is introduced with the desired spatial symmetries. For Rayleigh numbers between 9000 and 25000, the motion typically becomes time-periodic in a time of order τ_d. Integrating until $2{\cdot}25\tau_d$, there are about four cycles of periodic motion after the initial transient decays. In table 4 we give the periods for the standing-wave simulations and compare them with the experimental values obtained by Willis & Deardorff (1970).

It was pointed out in § 3 that the standing-wave solutions are unstable with respect to travelling-wave solutions. Willis & Deardorff observed both standing and travelling waves in their experiments. However, it should be pointed out that in their experiments both waveforms were of an intermittent character (both spatially and

Rayleigh number	X	Y	Calculated period	Experimental period (Willis & Deardorff 1970)
9000	3·55	2·48	0·270	0·28
12000	3·69	2·59	0·255	0·26
16000	3·81	2·66	0·229	0·21
20000	3·90	2·73	0·220	0·20
25000	4·00	2·80	0·230	0·19

TABLE 4. Periods of standing-wave solutions

temporally), and for this reason it is difficult to relate the instability of standing waves in our simulations to their experiments. Nevertheless, both the travelling- and the standing-wave solutions have periods that are in reasonably good agreement with the periods reported by Willis & Deardorff.

Next, we report a series of long simulations (through $38\tau_d$) for Rayleigh numbers 6500, 9000, 10000, 12000, 15000, 25000 and 30000, with the goal of isolating the threshold for broadband frequency components and the role of symmetry-breaking modes in producing these components. In the first series of simulations that we shall discuss, nearly steady two-dimensional rolls are generated with their axes parallel to the y-axis, and a finite-amplitude three-dimensional disturbance that breaks both the y-symmetry and spectral parity is then introduced. Contour plots of the velocity and temperature fields reveal complex spatial patterns after three thermal diffusion times. However, by the end of the simulations travelling-wave patterns emerge. In figure 2, we plot isotachs of w in the middle of the convection layer ($z = 0$). These contours are made on the last time step of each simulation (which corresponds to different points in the oscillation cycle for each case). It should be noted that the plot for $Ra = 6500$ differs from the others in that it exhibits antisymmetry for translations by $\frac{1}{2}X$ in the x-direction (the vertical direction on the plot). This indicates that the modes that violate spectral parity decay at $Ra = 6500$. However, at $Ra = 9000$ and the higher Rayleigh numbers spectral parity is broken.

In figure 3, we plot the time series for the y-component of velocity v at the point $x = \frac{1}{4}X$, $y = \frac{1}{4}Y$ and $z = 0{\cdot}354$ for the last six thermal diffusion times of the long ($38\tau_d$) simulations (with the exception of figure 3(f), which represents the last four thermal diffusion times for the simulation with $Ra = 25000$). The other components of velocity and the temperature at various points in the middle of the layer ($z = 0$) do not always contain all of the major frequencies (e.g. at $Ra = 6500$ the odd frequency harmonics are not present for the u and w velocity components or temperatures recorded in the middle of the layer). However, it appears that every significant frequency that appears in the other dynamical variables also appears in the spectrum of v, so we concentrate attention on this latter spectrum. Notice that the flows at $Ra = 6500$ and 10000 are both time-periodic, while those at the other Rayleigh numbers are more complex. We do not understand completely why the run at $Ra = 10000$ is less random than that at $Ra = 9000$, but it may be related to the roll re-orientation that is observed at $Ra = 12000$ (see below). In figure 4 we plot the frequency power spectra for the same y-velocity component over the second half of the long simulations (i.e. $19\tau_d$). By using only the second half of the time records,

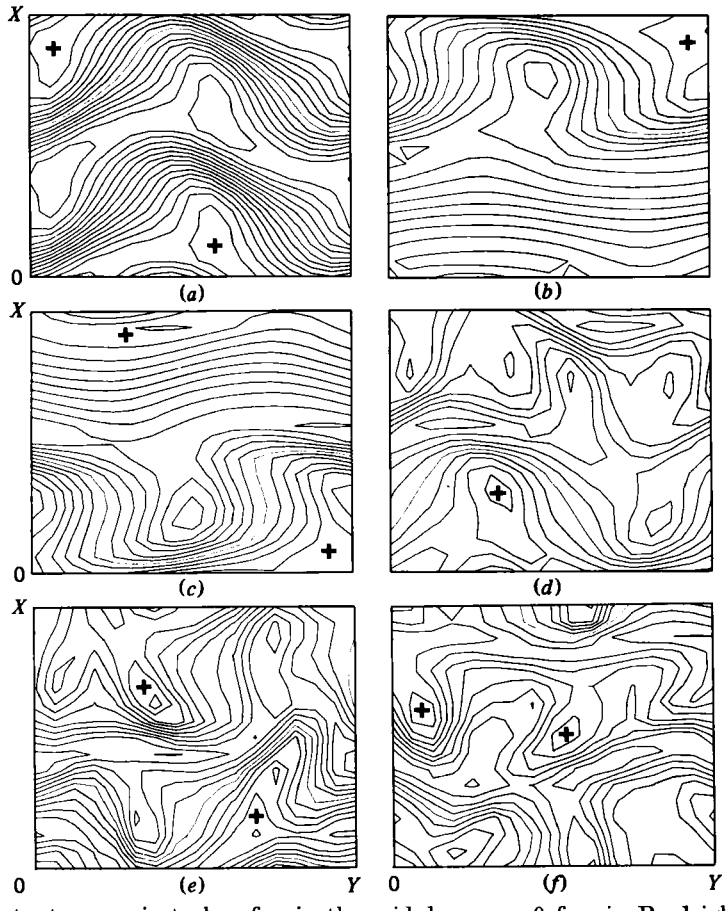

FIGURE 2. Instantaneous isotachs of w in the midplane $y = 0$ for six Rayleigh numbers. (*a*) $Ra = 6500$; (*b*) 9000; (*c*) 10000; (*d*) 12000; (*e*) 15000; (*f*) 25000. The + signs indicate regions of positive w.

it is possible to eliminate most transient effects on the spectrum. If one estimates a typical time scale for the time-dependence of the flows from the frequency at which the power spectrum has a maximum, one finds that the second half of the time records typically contain seventy or eighty oscillation periods. The low-frequency distortion in the spectra is produced by the convolution function used to eliminate the discontinuity between the beginning and end of the time series. Note that it is the logarithm of the power spectrum that is plotted in figure 4.

It should be noted that, while the relation $Y = 0{\cdot}7X$ is used for the simulations with $Ra = 6500$, 9000, 10000 and 25000, $Y = X$ is used for the simulations at $Ra = 12000$ and 15000. This choice was motivated by the fact that, when we used the relation $Y = 0{\cdot}7X$ for a long-time simulation at $Ra = 12000$, the rolls simply flip over by 90° (so they are aligned with the X-axis) and periodic motion ensues. Although there is a fairly wide dispersion in the roll wavelengths observed by Willis & Deardorff (1970), it seems reasonable to demand that the rolls have the mean experimental wavelength; by setting $Y = X$ one ensures that this will be true. Lipps (1976) used the same procedure in his simulation at $Ra = 25000$.

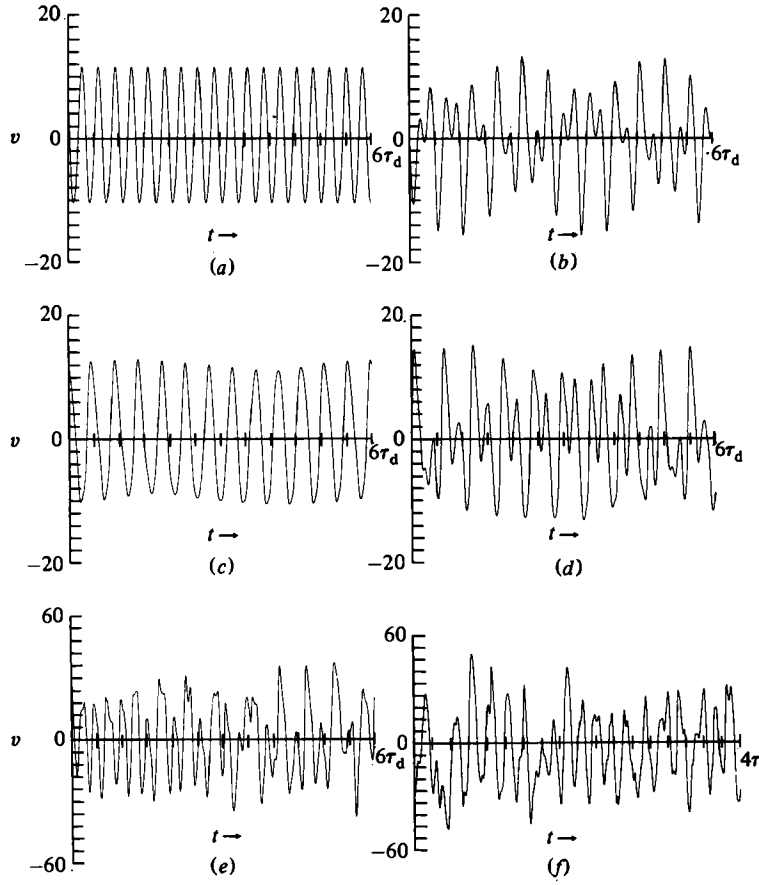

FIGURE 3. Time evolution of the velocity component $v(\frac{1}{4}X, \frac{1}{4}Y, \frac{1}{4}\sqrt{2}, t)$ for runs with resolution $M = N = 8$, $P = 16$ at various Rayleigh numbers over the last $6\tau_d$ of the runs for (*a*)–(*e*) and for the last $4\tau_d$ for (*f*). (*a*) $Ra = 6500$; (*b*) 9000; (*c*) 10000; (*d*) 12000; (*e*) 15000; (*f*) 25000.

The power spectrum shown in figure 4(*a*) reveals two distinct frequencies. The largest peak corresponds to a period equal to $0{\cdot}31\tau_d$; and three harmonics of this peak are visible in the graph. Willis & Deardorff (1970) report a period equal to $0{\cdot}32\tau_d$ for $Ra = 6500$. The good agreement may be fortuitous because of the uncertainty in the choice of Y and because of the experimental difficulty of observing the oscillations at Rayleigh numbers close to the oscillatory threshold. The second distinct frequency in figure 4(*a*) corresponds to a period equal to $0{\cdot}086\tau_d$, and one beat frequency between the two basic frequencies is visible. The major peak is 350000 times larger than the peak corresponding to the second frequency. For this reason, it is impossible to detect the second frequency in the time-evolution plot given in figure 3(*a*).

The results for $Ra = 9000$ plotted in figure 4(*b*) differ from those for $Ra = 6500$ in that there are broadband components. The spectrum at 9000 contains three distinct major peaks corresponding to periods equal to $1{\cdot}13\tau_d$, $0{\cdot}480\tau_d$ and $0{\cdot}256\tau_d$. The latter peak is the largest of the three, and agrees well with the value $0{\cdot}27\tau_d$ found by Willis & Deardorff. Lipps (1976) detected two distinct frequencies in his simulation at $Ra = 9000$, and estimated their values to be $0{\cdot}24\tau_d$ and $0{\cdot}45\tau_d$. It should be noted

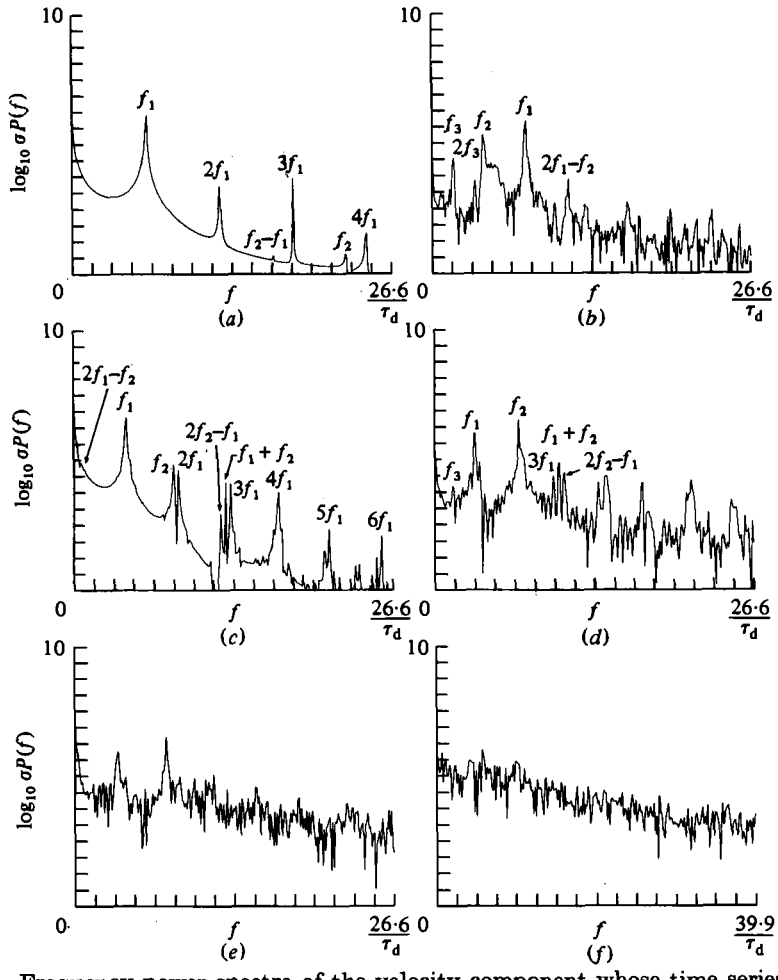

FIGURE 4. Frequency power spectra of the velocity component whose time series is plotted in figure 3. The spectra obtained using data from the last $19\tau_d$ of the runs ($12\tau_d$ for (f)). (a) Ra = 6500; (b) 9000; (c) 10000; (d) 12000; (e) 15000; (f) 25000.

that his solutions were obtained for a somewhat different value of Y than ours, and this may account for the discrepancy.

The spectrum for Ra = 10000 given in figure 4(c) reveals two distinct peaks. However, the plot given in figure 3(c) shows that the motion is time-periodic. Specifically, the waveform repeats itself exactly every eleven cycles of the fast oscillation. This is confirmed by inspection of the data used to generate the graph. (See also the Poincaré map for this run given in figure 6 below and the phase-space portrait in figure 11 below.)

Figures 4(d–f) reveal a progression to broader spectra as the Rayleigh number is increased to 25000. This is consistent with the experimental observations of Willis & Deardorff. The contour plots in figure 2 show that spectral parity is broken for all the Rayleigh numbers above 6500.

In order to determine the role of the symmetry-breaking modes in the production of broadband frequency components, the simulations at Ra = 9000 and 15000 were repeated with the modes that violate the spectral-parity condition given in (3.8) and

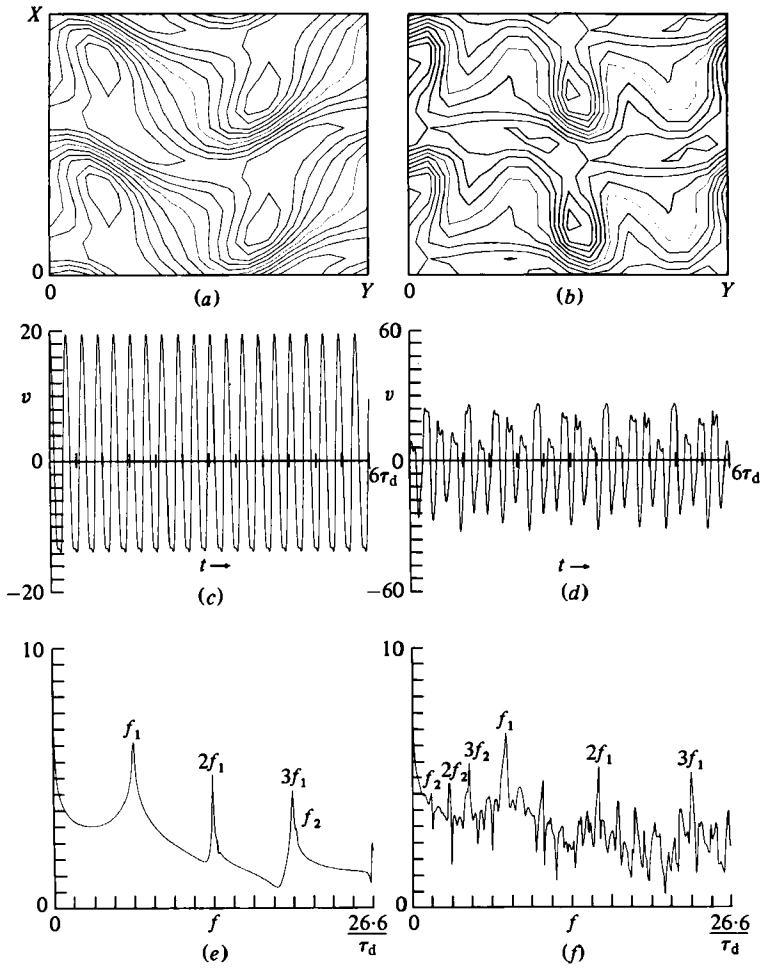

FIGURE 5. Runs with spectral parity enforced. (*a*), (*c*), (*e*): $Ra = 9000$. (*b*), (*d*), (*f*): $Ra = 15000$. Isotachs of w in the midplane $z = 0$: (*a*), (*b*). Time series of $v(\frac{1}{4}X, \frac{1}{4}Y, \frac{1}{4}\sqrt{2}, t)$: (*c*), (*d*). Frequency spectra of v over the last 19 τ_d: (*e*), (*f*).

(3.9) set equal to zero. The results are shown in figure 5. The isotachs of w plotted in figure 5(*a*) show that spectral parity holds because of the antisymmetry with respect to translations by $\frac{1}{2}X$ in the x-direction (along the ordinate in the graph). This translational antisymmetry appears in the data for the velocity components and temperature at points separated by $\frac{1}{2}X$ in the x-direction in the plane $z = 0$. Although the time series in figure 5(*b*) is not quite periodic, it is much less chaotic than the series shown in figure 3(*e*). It is clear that one can seriously underestimate the threshold for chaotic behaviour if one uses simulations in which spectral parity is imposed. A more important conclusion that can be drawn from the results plotted in figure 5 is that the symmetry-breaking modes are the cause of, rather than the result of, the onset of chaos. This result is not obvious *a priori* because it is conceivable that the symmetrized solutions could have a threshold for chaotic motion at the observed threshold, and that, once in a state of chaotic motion, they could destabilize the symmetry-breaking modes, thus drawing them into the motion.

Lipps (1976) has made an interesting observation which may help to interpret the

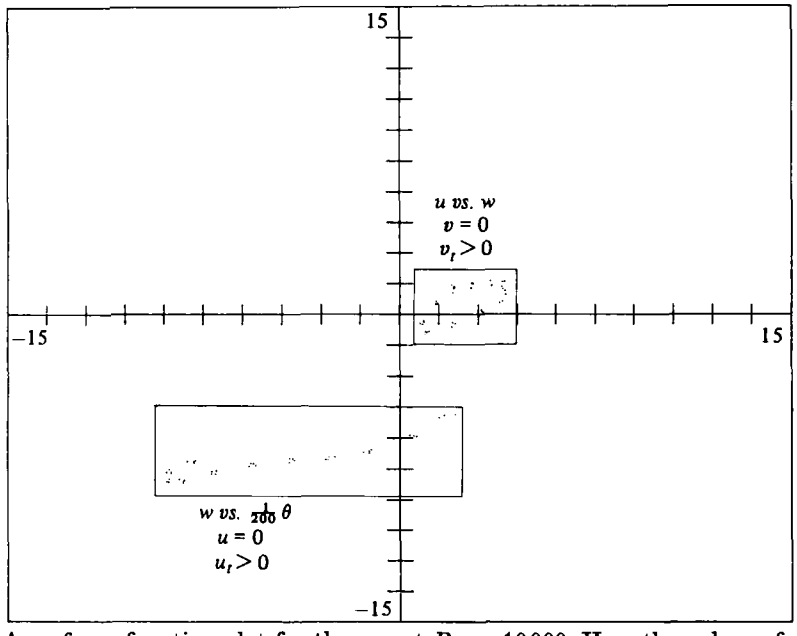

FIGURE 6. A surface-of-section plot for the run at $Ra = 10000$. Here the values of w and θ at $x = \frac{1}{4}X$, $y = z = 0$ are plotted at those times when $u(0, 0, 0) = 0$ with $\partial u/\partial t > 0$. This plot also includes the surface of section in which $u(0, 0, 0)$ is plotted *vs.* $w(\frac{1}{4}X, 0, 0)$ at those instants when $v(\frac{1}{4}X, \frac{1}{4}Y, \frac{1}{4}\sqrt{2}) = 0$ with $\partial v/\partial t > 0$. This plot was made using data from the last 19 τ_d of the run.

role of the modes that break spectral parity in generating new frequencies in the flow. He pointed out that, in his simulation at $Ra = 9000$, travelling-wave disturbances on adjacent rolls had different strengths and, as a consequence, travelled at different speeds. The fact that the disturbances had different strengths on adjacent rolls implies that spectral parity was also broken in his simulation (i.e. the velocity components and temperature are no longer symmetric or antisymmetric with respect to translations by $\frac{1}{2}X$ in the x-direction). It appears that the symmetry-breaking modes produce a modulation of the rolls which produces a new frequency in the flow. Since according to the Ruelle–Takens theory it is unusual to find a quasiperiodic flow with more than two distinct frequencies, the role of symmetry-breaking modes in producing new frequencies is important in the generation of early chaos.

In figure 6, we give two surface-of-section plots (Poincaré maps) at $Ra = 10000$. In one surface of section we plot the values of w and θ at $x = \frac{1}{4}X$, $y = 0$, $z = 0$ at those instants when $u = 0$ with $\partial u/\partial t > 0$ at $x = y = z = 0$. In the other surface-of-section plot included in figure 6, we plot the values of $u(0, 0, 0, t)$ *vs.* $w(\frac{1}{4}X, 0, 0, t)$ when $v = 0$ with $\partial v/\partial t > 0$ at $x = \frac{1}{4}X$, $y = \frac{1}{4}Y$, $z = 2/4$. Apparently, when $Ra = 10000$, the points of the surfaces of section are a finite number of discrete points, attesting to the periodic nature of the flow. On the other hand, the surface-of-section plot given in figure 7 at $Ra = 15000$ indicates a random orbit in the sense that the points are scattered in an apparently random and chaotic way. In this latter figure, the values of w and θ are plotted at $x = \frac{1}{4}X$, $y = z = 0$ at those instants of time when $u(0, 0, 0, t) = 0$ and $\partial u/\partial t > 0$.

In figures 8–12 we plot projections of the time-dependent orbits on two-dimensional phase planes. When $Ra = 6500$ the orbits are clearly time-periodic (see figure 8). In

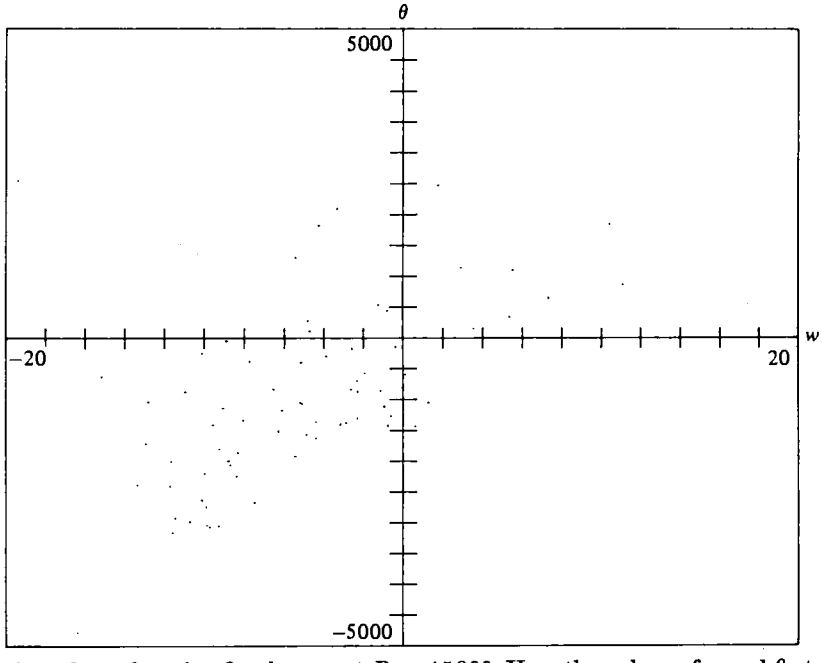

FIGURE 7. A surface of section for the run at $R = 15000$. Here the values of w and θ at the point $x = \frac{1}{2}X$, $y = z = 0$ are plotted at those instants when $u(0, 0, 0, t) = 0$ with $\partial u/\partial t > 0$. Observe the chaotic character of this orbit. This plot was made using data from the last $19\tau_d$ of the run.

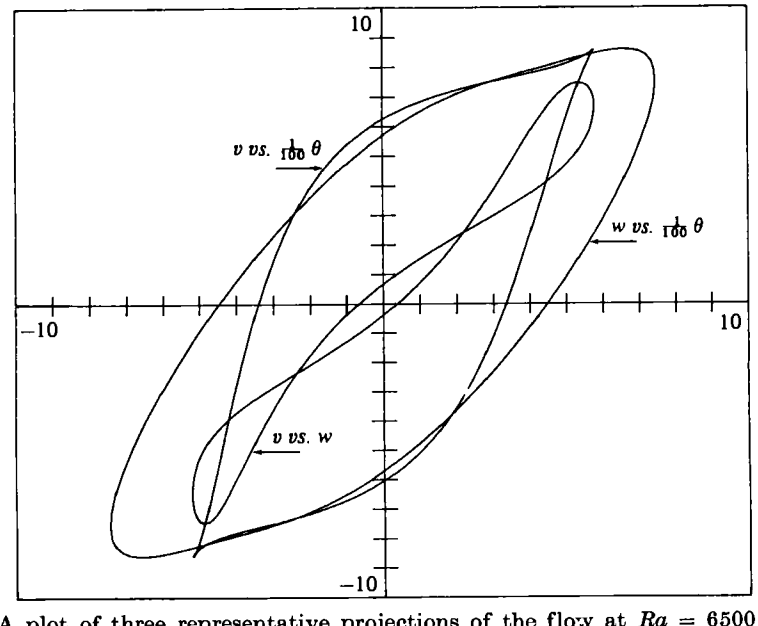

FIGURE 8. A plot of three representative projections of the flow at $Ra = 6500$ onto a two-dimensional phase space. Observe the periodic character of the flow. This plot is made using data from the last $6\tau_d$ of the run.

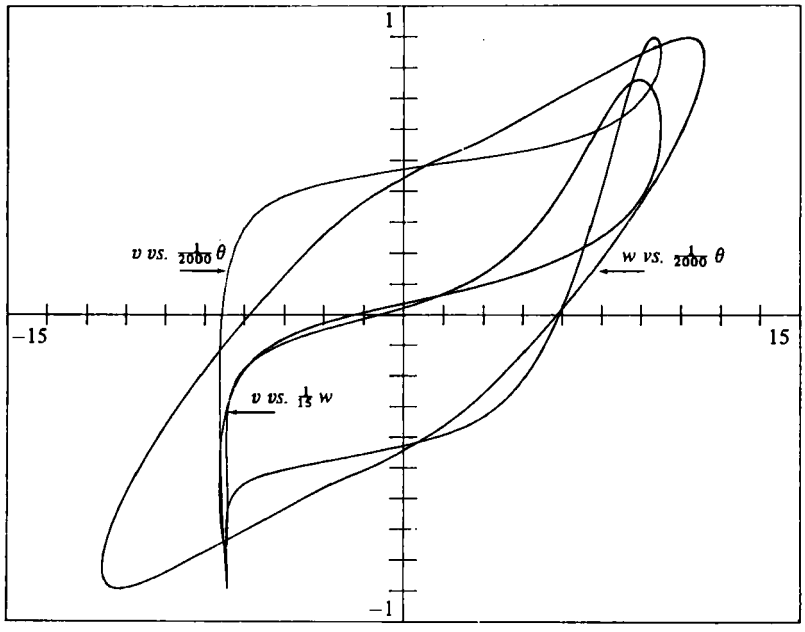

FIGURE 9. A plot of three representative projections of the flow at $Ra = 9000$ in which spectral parity is enforced. The projections are made onto a two-dimensional phase plane. Observe the periodic character of the flow. This plot is made using data from the last $6\tau_d$ of the run.

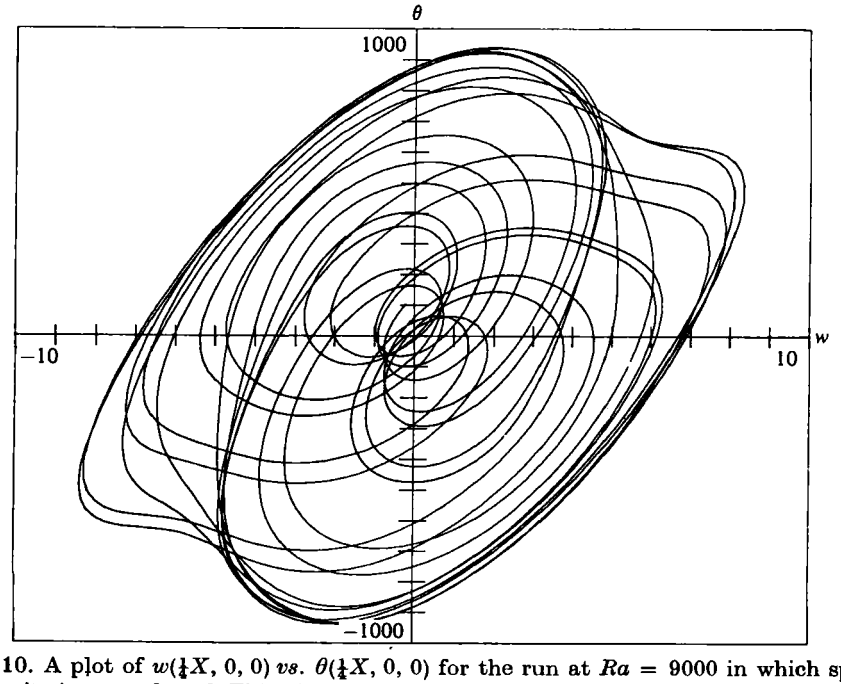

FIGURE 10. A plot of $w(\frac{1}{4}X, 0, 0)$ *vs.* $\theta(\frac{1}{4}X, 0, 0)$ for the run at $Ra = 9000$ in which spectral parity is not enforced. This plot is made using data from the last $6\tau_d$ of the run.

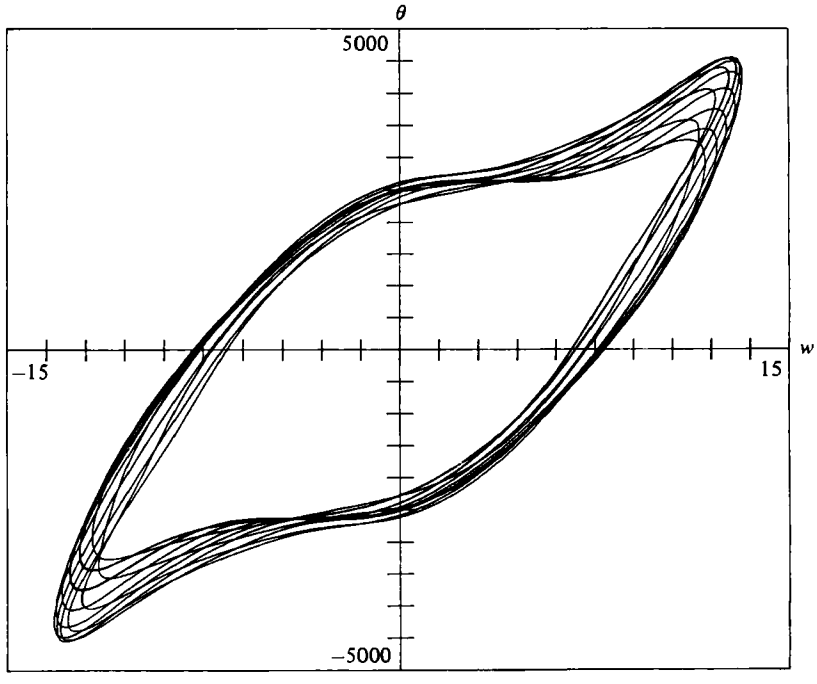

FIGURE 11. Same as figure 10 except at $Ra = 10000$.

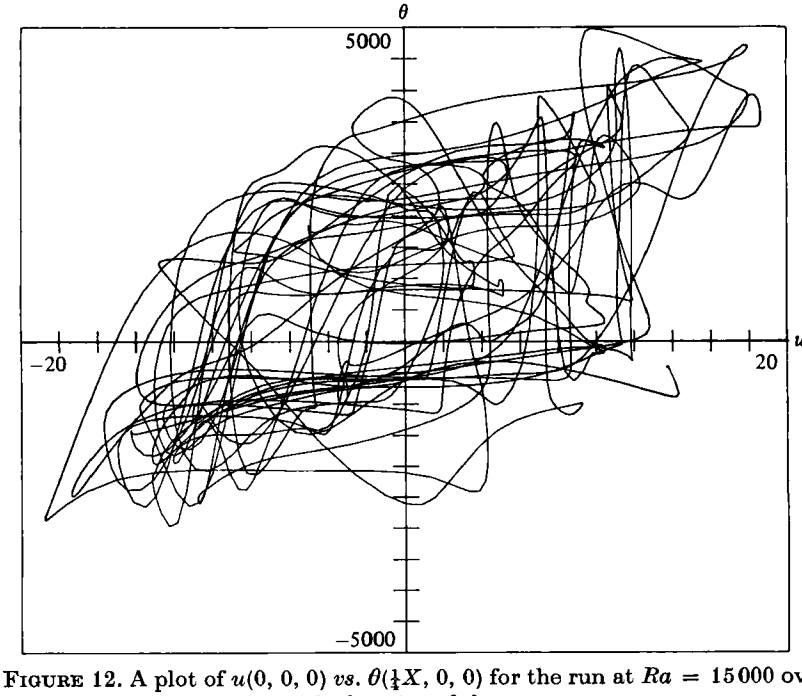

FIGURE 12. A plot of $u(0, 0, 0)$ *vs.* $\theta(\frac{1}{4}X, 0, 0)$ for the run at $Ra = 15000$ over the last $6\tau_d$ of the run.

figure 9, two-dimensional orbits are plotted for the run at $Ra = 9000$ with the spectral symmetries (see figure 4) imposed. Apparently this orbit is time-periodic. On the other hand, when the symmetries are not imposed the orbit at $Ra = 9000$ plotted in figure 10 shows some weakly strange behaviour, in which the orbit is not quite periodic and may be weakly chaotic. The orbit plotted in figure 11 at $Ra = 10000$ shows nearly periodic behaviour. Finally, the two-dimensional orbit plotted in figure 12 at $Ra = 15000$ shows the chaotic nature of this orbit.

In summary, our simulations of convection in air demonstrate periodic, quasi-periodic and chaotic behaviour in the range of Rayleigh numbers between 6500 and 25000. Our results appear to be consistent with the Ruelle–Takens theory in that simulated flows that contain three or more distinct frequencies also contain broadband frequency components.

We should like to thank Dr F. Lipps for helpful discussions and Professor O. Lanford for encouraging us to study surface-of-section plots. We should also like to thank Dr A. Patera for collaborating in the development of the computer codes used in this study. This work was supported by the National Science Foundation under Grant ATM-8017092, and the Office of Naval Research under Contracts N00014-77-C-0138 and N00014-79-C-0478, and the Army Research Office under Contract DAAG29-81-K-0025. The computations were performed at the Computing Facility of the Center for Atmospheric Research, which is supported by the National Science Foundation.

REFERENCES

Ahlers, G. & Behringer, R. P. 1978 *Phys. Rev. Lett.* **40**, 712–716.

Ahlers, G. & Behringer, R. P. 1979 *Prog. Theor. Phys. Suppl.* **64**, 186–201.

Busse, F. H. & Clever, R. M. 1979 *J. Fluid Mech.* **91**, 319–335.

Chirikov, B. V. 1959 *Atomnaya Energiya* **6**, 630.

Clever, R. M. & Busse, F. H. 1974 *J. Fluid Mech.* **65**, 625–645.

Clever, R. M. & Busse, F. H. 1978 *J. Appl. Math. & Phys.* **29**, 711–714.

Curry, J. H., Herring, J. R., Loncaric, J. & Orszag, S. A. 1982 Order and disorder in two and three dimensional Bénard convection. To be published.

Ford, J. & Lunsford, G. H. 1970 *Phys. Rev.* A **1**, 59–70.

Gollub, J. P. & Benson, S. H. 1980 *J. Fluid Mech.* **100**, 449–470.

Herbert, T. 1976 Periodic secondary motions in a plane channel. In *Proc. 5th Int. Conf. on Numerical Methods in Fluid Dynamics* (ed. A. I. van de Vooren & P. J. Zandbergen). Lecture Notes in Physics, vol. 59, p. 235. Springer.

Herbert, T. 1977 Finite amplitude stability of plane parallel flows. In *Laminar–Turbulent Transition, AGARD Conf. Proc. no.* 224, pp. 3-1–3-10.

Krishnamurti, R. 1973 *J. Fluid Mech.* **60**, 285–303.

Landau, L. D. & Lifschitz, E. M. 1959 *Fluid Mechanics*. Pergamon.

Lanford, O. 1982 In *Proc.* 1981 *Les Houches Summer School of Physics*. North-Holland.

Laufer, J. 1954 The structure of turbulence in fully developed pipe flow. *NASA Rep.* no. 1174.

Lipps, F. B. 1976 *J. Fluid Mech.* **75**, 113–148.

Marcus, P. S. 1981 *J. Fluid Mech.* **103**, 241–255.

McLaughlin, J. M. & Martin, P. C. 1975 *Phys. Rev.* A **12**, 186–203.

Newhouse, S., Ruelle, D. & Takens, F. 1978 *Commun. Math. Phys.* **64**, 35–40.

Orszag, S. A. 1971 *J. Fluid Mech.* **50**, 689.

Orszag, S. A. & Kells, L. C. 1980 *J. Fluid Mech.* **96**, 159–205.

Orszag, S. A. & Patera, A. T. 1981 Subcritical transition to turbulence in planar shear flows. In *Transition and Turbulence* (ed. R. E. Meyer), pp. 127–145. Academic.

Ruelle, D. & Takens, F. 1971 *Commun. Math. Phys.* **20**, 167–192.

Toomre, J., Gough, D. O. & Spiegel, E. A. 1977 *J. Fluid Mech.* **79**, 1–31.

Willis, G. E. & Deardorff, J. W. 1970 *J. Fluid Mech.* **44**, 661–672.

Willis, G. E., Deardorff, J. W. & Somerville, R. C. J. 1972 *J. Fluid Mech.* **54**, 351.